JOC The Journal of Organic Chemistry

Article

pubs.acs.org/joc

Theoretical Study of Nickel-Catalyzed Selective Alkenylation of Pyridine: Reaction Mechanism and Crucial Roles of Lewis Acid and Ligands in Determining the Selectivity

Vijay Singh,[†] Yoshiaki Nakao,[‡] Shigeyoshi Sakaki,*[,§] and Milind M. Deshmukh*[,†]

[†]Department of Chemistry, Dr. Harisingh Gour Central University, Sagar 470003, India

[‡]Department of Material Chemistry, Graduate School of Engineering, Kyoto University, Katsura, Nishikyo-ku, Kyoto 615-8510, Japan

[§]Fukui Institute for Fundamental Chemistry, Kyoto University, Nishihiraki-cho, Takano, Sakyo-ku, Kyoto 606-8103, Japan

Supporting Information

ABSTRACT: Selective alkenylation of pyridine is challenging in synthetic organic chemistry due to the poor reactivity and regioselectivity of the aromatic ring. We theoretically investigated Ni-catalyzed selective alkenylation of pyridine with DFT. The first step is coordination of the pyridine−$AlMe_3$ adduct with the active species $Ni^{(0)}(NHC)(C_2H_2)$ **1** in an η^2-fashion to form an intermediate **Int1**. After the isomerization of **Int1**, the oxidative addition of the C−H bond of pyridine across the nickel−acetylene moiety occurs via a transition state **TS2** to form a $Ni^{(II)}(NHC)$ pyridyl vinyl intermediate **Int3**. This oxidative addition is rate-determining. The next step is C−C bond formation between pyridyl and vinyl groups leading to the formation of vinyl-pyridine (**P1**). One of the points at issue in this type of functionalization is how to control the regioselectivity. With the use of Ni(NHC)/$AlMe_3$ catalyst, the C^4- and C^3-alkenylated products ($\Delta G^{\circ\ddagger}$ = 17.4 and 21.5 kcal mol^{-1}, respectively) are formed preferably to the C^2 one ($\Delta G^{\circ\ddagger}$ = 22.0 kcal mol^{-1}). The higher selectivity of the C^4-alkenylation over the C^3 and the C^2 ones is attributed to the small steric repulsion between NHC and $AlMe_3$ in the C^4-alkenylation. Interestingly, with Ni($P(i\text{-}Pr)_3$)/$AlMe_3$ catalyst, the C^2-alkenylation occurs more easily than the C^3 and C^4 ones. This regioselectivity arises from the smaller steric repulsion induced by $P(i\text{-}Pr)_3$ than by bulky NHC. It is notable that $AlMe_3$ accelerates the alkenylation by inducing the strong CT from Ni to pyridine−$AlMe_3$. In the absence of $AlMe_3$, pyridine strongly coordinates with the Ni atom through the N atom, which increases Gibbs activation energy ($\Delta G^{\circ\ddagger}$ = ∼27 kcal mol^{-1}) of the C−H bond activation. In other words, $AlMe_3$ plays two important roles, acceleration of the reaction and enhancement of the regioselectivity for the C^4-alkenylation.

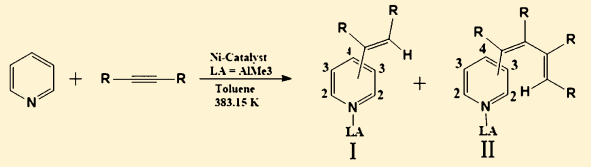

Catalyst	C^2	C^3	C^4
Ni(NHC)/$AlMe_3$	Difficult	Minor (I)	Major (I)
Ni($P(i\text{-}Pr)_3$)/$AlMe_3$	Major (II)	Difficult	Minor (II)
Ni(NHC) without LA	Difficult	Difficult	Difficult

INTRODUCTION

Pyridine is one of the important chemicals for synthesis of large numbers of derivatives which are useful in pharmaceutics,[1] natural products,[2] and optical materials.[3] Thus, functionalization of pyridine is extremely important in synthetic chemistry. However, the direct functionalization of pyridine remains a significant challenge due to low reactivity and poor chemo- and regioselectivity of the aromatic ring.[4] For instance, electrophilic substitution reaction of pyridine such as Friedel−Crafts and halogenation is not effective, in general. To utilize pyridine ring, we need to introduce substituent(s) on the ring[5] through some other reaction.[6] As a good candidate for such a reaction, functionalization through the direct C−H bond activation of aromatic ring with transition metal catalyst has gained significant attention, recently.[7] Murakami and co-workers[8] successfully applied the C−H activation procedure to a novel regio- and stereoselective alkenylation reaction of pyridine using ruthenium catalyst. Bergman, Ellman, and co-workers[9] also reported Rh(I)-catalyzed alkenylation of pyridine at the C^2-position. Instead of precious **4d** metals, more abundant Ni was successfully applied to the direct arylation of pyridine and quinoline by Tobisu, Chatani, and co-workers.[10] However, we still find harsh reaction conditions,[11] limited scope of substrate,[12] need of a directing group as substituent on the pyridine ring,[13] and N-substituted oxide[14] in many functionalization reactions. Further, it should be noted that the C^2−H bond activation generally occurs due to the proximity effect of pyridine N atom which coordinates with metal as a Lewis base.[15]

In contrast to the C^2-functionalization, the direct C^3- and C^4-functionalizations of pyridine have been scarcely reported except for several pioneering works.[16−22] For instance, Ong and co-workers[17] and Nakao group[18] first succeeded in the selective C^4-alkenylation using Ni(NHC)/Lewis acid cooperative catalyst (NHC = *N*,*N*-diphenyl *N*-heterocyclic carbene). They also reported direct evidence that a bimetallic η^2-η^1-pyridine nickel

Received: October 1, 2016
Published: December 14, 2016

DOI: 10.1021/acs.joc.6b02394
J. Org. Chem. 2017, 82, 289−301

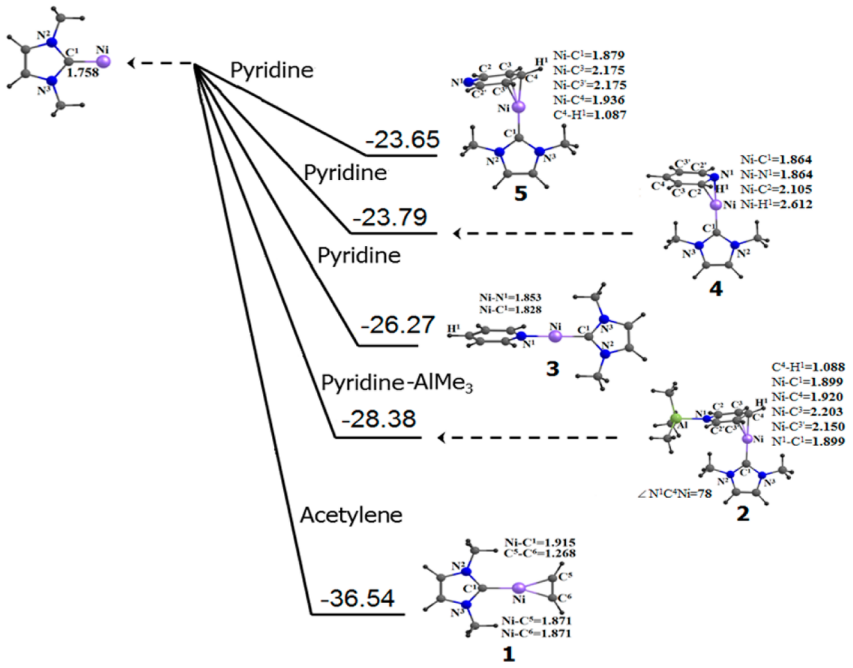

Figure 1. Geometries and Gibbs energies by coordination of various molecules with Ni(NHC). The B3LYP-D3/BS-II method was used.

aluminum species is formed prior to the C−H bond activation.[17] Yu and co-workers reported the selective C^3-functionalization of pyridine by palladium catalyst.[19] Stronger trans-influence of bipyridine ligand was suggested to be crucial for the selective C^3-functionalization. Shi and Li reported highly C^3-selective iridium-catalyzed addition reaction of aromatic aldehydes to pyridine in the presence of triethylsilane.[20] In this reaction, the oxidative addition of the C^3−H bond of pyridine to a silyliridium species affords a hydride(3-pyridyl)(silyl)iridium species followed by reaction with aldehyde to form the C^3-substituted product. Kanai, Matsunaga, and co-workers reported the direct C^4-alkenylation of pyridine by $CoBr_2$/$LiBEt_3H$ catalyst.[21] They suggested that the Et_3B species is crucial to improve the C^4-selectivity by suppressing reaction at the C^2-site. Suginome and Ohmura reported the selective addition of silyl boronic ester to pyridine in the presence of a palladium catalyst to give *N*-boryl-4-silyl-1,4-dihydropyridine in high yield.[22] The first step is oxidative addition of silylboronic ester to Pd(0), the next step is regioselective insertion of pyridine into the Pd−boryl bond, and the final step is reductive elimination of a silylated dihydropyridine product.

Among various reports, the direct addition of alkenes and alkynes to pyridine with a nickel/Lewis acid cooperative catalyst reported by Nakao, Hiyama, and co-workers[15,16,18] is considerably interesting because the selectivity can be controlled well by appropriate combination of ligand and Lewis acid (LA). For instance, (i) nickel/P(*i*-Pr)$_3$/Lewis acid (such as $ZnMe_2$ or $AlMe_3$) promotes the C^2-alkenylation.[15] (ii) The combination of nickel/NHC with $AlMe_3$ mainly allows the direct C^4-alkenylation, where the C^3-alkenylated pyridine is produced as a minor product. (iii) The use of a very bulky (2,6-*t*Bu$_2$-4-Me-$C_6H_2O)_2AlMe$ (MAD) Lewis acid exclusively allows the C^4-functionalization. And (iv) the C^2-functionalization occurs preferably in the absence of LA. In their studies, we found many interesting questions to be answered. The first question is the reaction mechanism of this direct functionalization reaction. Recently, Ni-catalyzed direct alkylation of benzene was reported by Eisenstein, Hartwig, and co-workers, in which direct H transfer from benzene to alkene was proposed.[23] In Ni-catalyzed decyanative [4 + 2] cycloaddition in the presence of LA, on the other hand, the C−C σ-bond activation occurs via usual concerted oxidative addition to Ni(0) center.[24] Apart from these, various other possible mechanisms of the C−H bond activation or metal mediated H atom transfer reactions were nicely summarized by Hall et al.[25a] and also by Ess and Goddard[25b]. It is of considerable interest to investigate through which of the H transfer and the concerted oxidative addition mechanism pyridine C−H bond activation occurs. More important is to elucidate the roles of LA in controlling the regioselectivity. Theoretical answers to these questions are indispensable for achieving further development of this catalytic system.

In this theoretical study, we investigated regioselective alkenylation of pyridine catalyzed by Ni(0) complex combined with *N*,*N*-diphenyl *N*-heterocyclic carbene (NHC) as ligands and $AlMe_3$ as a Lewis acid. The effect of triisopropylphosphine P(*i*-Pr)$_3$ ligand was also explored. Our purposes here are to clarify the reaction mechanism of this alkenylation reaction, uncover the characteristic features of all elementary steps, elucidate the role of the Lewis acid ($AlMe_3$), and explain the reasons for experimentally observed regioselectivity.

COMPUTATIONAL DETAILS

Geometries of all species studied in this work were optimized by the DFT method with the B3PW91 functional.[26,27] Basis set systems of two kinds, BS-I and BS-II, were used in this work. In BS-I, the 6-31G(d) basis set[28] was employed for H, C, N, P, and Al atoms and the LANL2DZ basis set was employed for Ni atom with effective core potentials (ECPs) for its core electrons.[29] In BS-I, one set of p-polarization function was added to a reactive H atom of pyridine which participates in the C−H bond activation. This BS-I was employed for geometry optimization and evaluation of vibrational frequencies. The vibrational frequencies were calculated to check whether the optimized geometry is an equilibrium structure or a transition state. In a better basis set system BS-II, a (311111/22111/411/1) basis set by the Stuttgart−Dresden−Bonn (SDD) group was employed for Ni with ECPs for the core electrons.[30] For H, C, N, P, and Al atoms, 6-311+G(d) basis sets were used, where

DOI: 10.1021/acs.joc.6b02394
J. Org. Chem. 2017, 82, 289−301

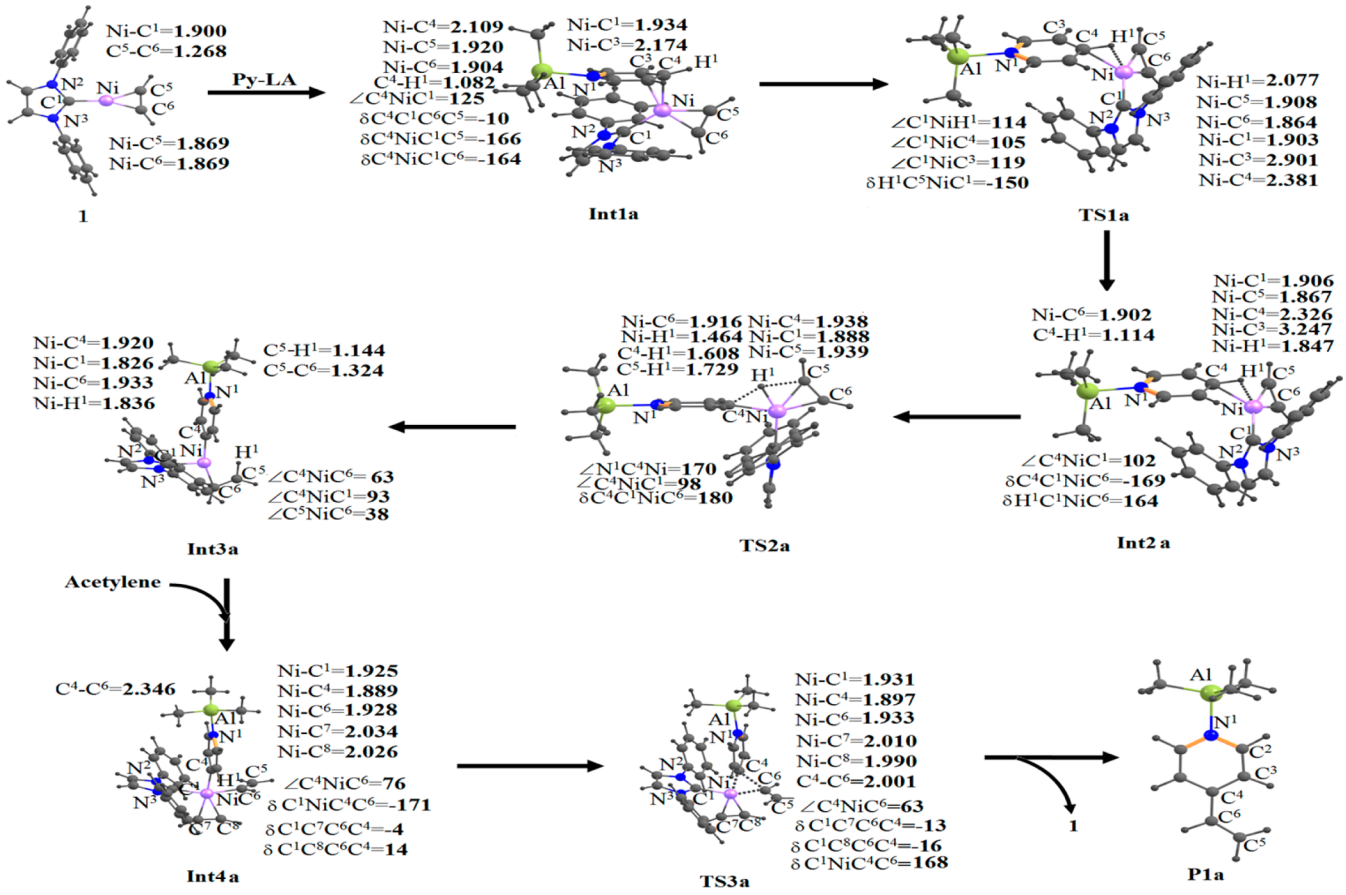

Figure 2. Geometrical changes in the C^4-alkenylation of pyridine by the Ni(NHC)/$AlMe_3$ catalyst leading to the formation of *p*-vinyl pyridine−$AlMe_3$ **P1a**. Distances are given in angstroms, and angles are in degrees.

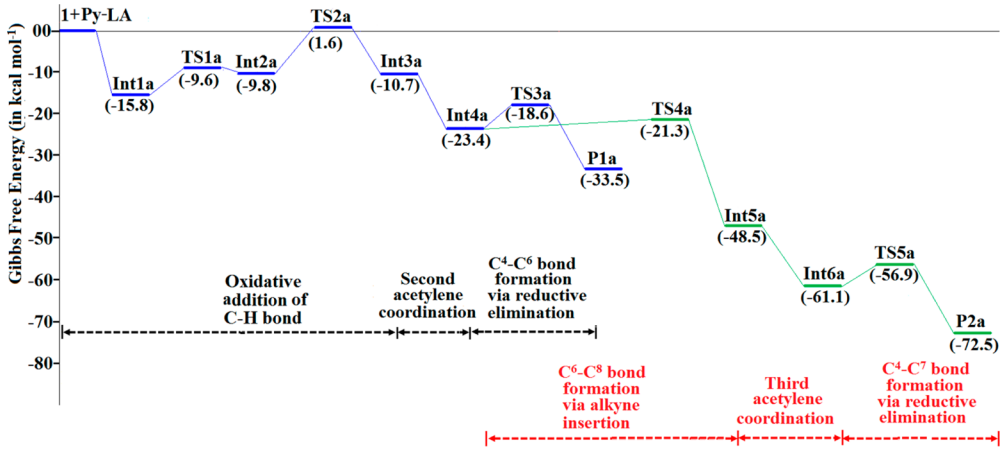

Figure 3. Gibbs energy changes (kcal mol^{-1}) in the C^4-alkenylation of pyridine by the Ni(NHC)/$AlMe_3$ catalyst. The B3LYP-D3/BS-II method was used.

one set of p-polarization functions was added to a reactive hydrogen atom of pyridine.[28a] The energy and population changes were calculated with the B3LYP-D3 functional[31a] employing BS-II, where the geometries optimized by the DFT/BS-I were employed. We wish to mention that B3LYP-D3/BS-II//B3PW91/BS-I presents similar energy changes to those by B3LYP-D3/BS-II//B3LYP-D3/BS-I, and the use of the B3LYP-D3/BS-II//B3PW91/BS-I method is reasonable in a practical sense;[31b] see page S24 in the Supporting Information. Also we checked the basis set effects to examine if the BS-II presents reliable results;[31c] see page S25 in Supporting Information. The natural bond orbital (NBO) population analysis was made in order to investigate the population changes in reaction. All calculations were performed with the Gaussian 09 program package including NBO analysis version 3.1.[32] The solvent effect of toluene was evaluated by the conductor-like polarizable continuum model (CPCM).[33a−c] Thermal corrections and entropy contributions of vibrational movements to the Gibbs energy change were evaluated at the B3PW91/BS-I level at 383.15 K and 1 atm, where the solvation effect was evaluated with the CPCM model. The Gibbs energy was used for the discussion, where the translational entropy was corrected with the method developed by Whitesides et al.[33d] The reaction temperature was set to 383.15 K to mimic the experimental conditions.

DOI: 10.1021/acs.joc.6b02394
J. Org. Chem. 2017, 82, 289−301

Scheme 1. Catalytic Cycle for Alkenylation of Pyridine by the Ni(NHC)/$AlMe_3$ Catalyst, Leading to the Formations of Vinyl Pyridine−$AlMe_3$ P1 and Butadienyl Pyridine−$AlMe_3$ P2

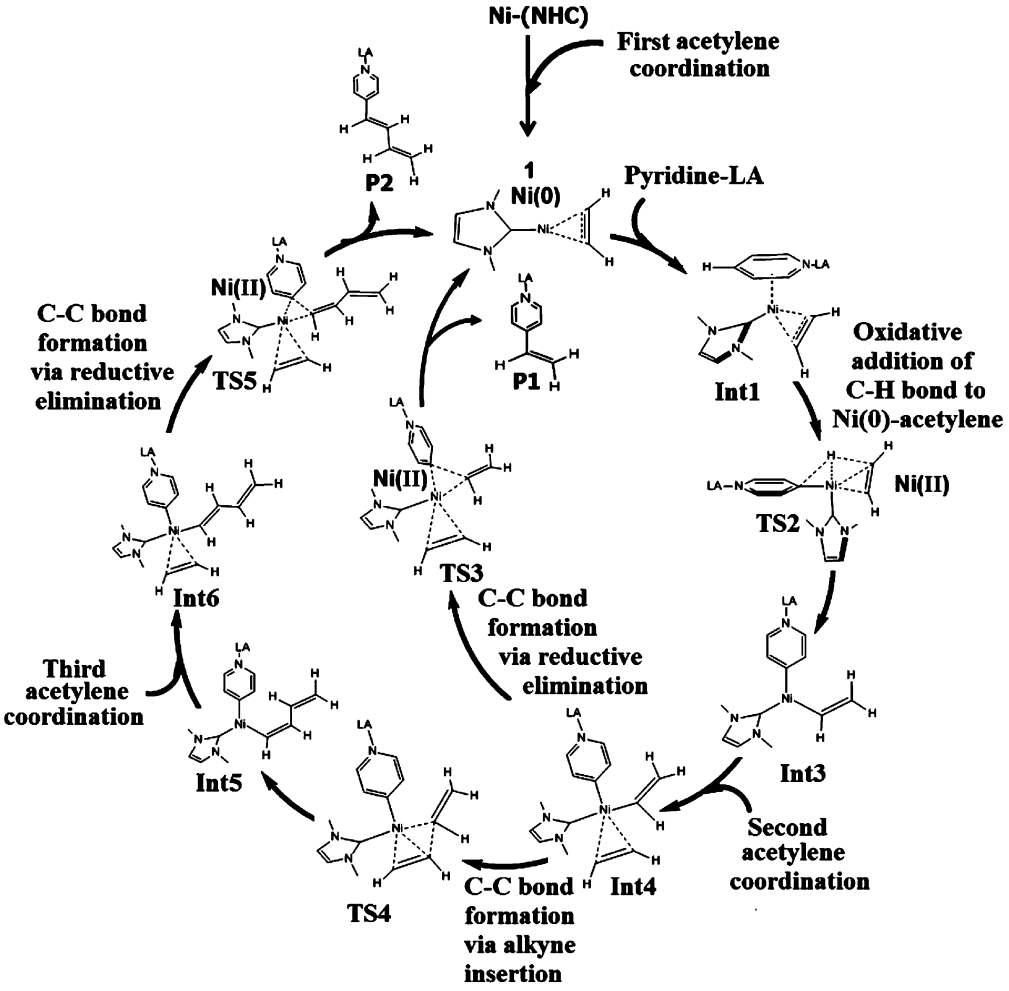

RESULTS AND DISCUSSION

Before starting theoretical study of the reaction mechanism, we first elucidated what an active species is. Considering that NHC is a strong ligand, we investigated here various complexes of Ni(NHC) with pyridine, pyridine−$AlMe_3$, and acetylene. Their optimized geometries are shown in Figure 1 with Gibbs energies. As can be seen in Figure 1, pyridine−$AlMe_3$ coordination with the Ni(0) atom is moderately more stable than pyridine coordination by about 2 to 5 kcal mol^{-1}. Among all the complexes examined, the acetylene complex Ni(NHC)(C_2H_2) **1** is substantially more stable than the pyridine (by ∼10 kcal mol^{-1}) and pyridine−$AlMe_3$ (by ∼8 kcal mol^{-1}) complexes. These results suggest that the reaction starts from **1**.

Catalytic Cycle for C^4-Alkenylation of Pyridine with Ni(NHC)/$AlMe_3$ Catalyst: Geometry and Energy Changes. Figures 2 and 3 present geometry and energy changes in the C^4-alkenylation by Ni(NHC)/$AlMe_3$, respectively. It is likely that the first step of the catalytic cycle is coordination of the pyridine−$AlMe_3$ adduct with the active species **1** to form an intermediate Ni(NHC)(C_2H_2)($C_5NH_5AlMe_3$) **Int1a**; see Scheme 1. The stabilization energy of **Int1a** is −15.8 kcal mol^{-1} (Figure 3). In **Int1a**, one C−C bond of pyridine ring interacts with the Ni atom in an η^2-fashion. The Ni−C^3 and Ni−C^4 distances are similar (2.174 and 2.109 Å, respectively), and the C^4−H bond moderately deviates from the pyridine plane, while its C^4−H bond distance (1.082 Å) is similar to the other C−H bond distances. **Int1a** isomerizes to **Int2a** via transition state **TS1a**. In **Int2a**, the C^4−H bond coordinates with the Ni atom, where the C^4−H bond is somewhat elongated and the Ni−C^4 bond is substantially elongated to 1.114 and 2.326 Å, respectively. The Gibbs activation energy ($\Delta G^{\circ\ddagger}$) of this process is moderate (6.2 kcal mol^{-1} relative to **Int1a**), indicating that this process easily occurs. Starting from **Int2a**, the C^4−H bond activation occurs through a transition state **TS2a** to afford a nickel vinyl pyridyl intermediate, Ni(NHC)($CHCH_2$)($C_5NH_4AlMe_3$) **Int3a**. **TS2a** is not a usual transition state of concerted oxidative addition but seems to be a transition state for H^1-transfer from pyridine−$AlMe_3$ to acetylene. Though the short Ni−H^1 (1.464 Å) and Ni−C^4 (1.938 Å) distances and the considerably long C^4−H distance (1.608 Å) are similar to those of the transition state of the concerted oxidative addition, the rather short C^5−H distance (1.729 Å) suggests that the H^1 atom starts to interact with the C^5 atom of acetylene. The $\Delta G^{\circ\ddagger}$ value is 17.4 kcal mol^{-1} relative to **Int1a** and 11.4 kcal mol^{-1} relative to **Int2a** (Figure 3). The intermediate **Int3a** is moderately more stable than **Int2a** by 1.0 kcal mol^{-1}. In **Int3a**, the C^5−H distance (1.144 Å) is longer than the other C−H bond and the Ni−H distance (1.836 Å) is short, suggesting the presence of agostic interaction between the C^5−H bond and the Ni atom. On the other hand, Ni−C^1 (1.826 Å) and Ni−C^4 (1.920 Å) distances are similar to the normal Ni−C bond distance. These geometrical features indicate that **Int3a** is a

DOI: 10.1021/acs.joc.6b02394
J. Org. Chem. 2017, 82, 289−301

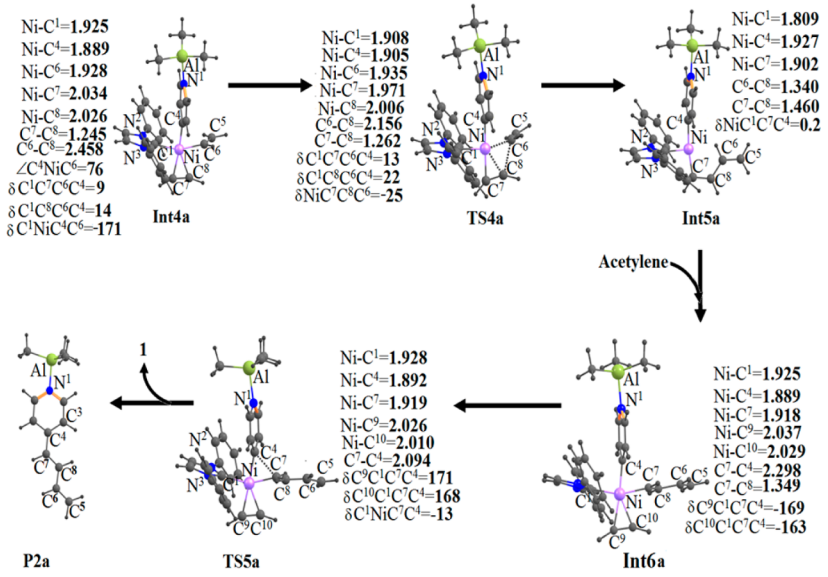

Figure 4. Geometrical changes in the C^4-alkenylation of pyridine by the Ni(NHC)/$AlMe_3$ catalyst leading to the formation of *p*-butadienyl pyridine–$AlMe_3$ **P2a**. Distances are given in angstroms, and angles are in degrees.

Ni(II) complex containing vinyl and pyridyl groups. Because the Ni oxidation state increases from 0 to II when going from **Int1a** to **Int3a**, this process is understood to be the oxidative addition of the pyridine C–H bond to a nickel–acetylene moiety,[34] which is different from the concerted oxidative addition of the C–H bond to a Ni(0) center.

The next step is coordination of one more acetylene to the Ni atom in **Int3a** to afford a nickel(II) acetylene complex Ni(NHC)($CHCH_2$)($C_5H_4NAlMe_3$)(C_2H_2) **Int4a**; see Scheme 1 and Figure 2. This is called the second acetylene coordination hereafter. This acetylene coordination is exergonic by −12.7 kcal mol^{-1}. Thus-formed intermediate **Int4a** undergoes the C^4–C^6 bond formation through reductive elimination. As seen in Figure 3, **TS3a** of this reaction is moderately less stable than **Int4a** by 4.8 kcal mol^{-1}. In **TS3a**, the C^4–C^6 bond distance becomes shorter (2.001 Å) but the Ni–C^4 and Ni–C^6 bond distances increase little, indicating that the C^4–C^6 bond formation is in progress in **TS3a** without the Ni–C^4 and Ni–C^6 bond weakening. From **TS3a**, the para-substituted vinyl-pyridine–$AlMe_3$ **P1a** is produced with the regeneration of active species **1**.[35] The total Gibbs activation energy ($\Delta G^{\circ\ddagger}$) and reaction energy (ΔG°) for the formation of **P1a** are 17.4 kcal mol^{-1} and −33.5 kcal mol^{-1}, respectively.

Another possible reaction is the C^6–C^8 bond formation starting from **Int4a**, which corresponds to acetylene insertion into the Ni–vinyl bond. This reaction occurs via a transition state **TS4a** to form a nickel(II) butadienyl intermediate Ni(NHC)-(C_4H_5)($C_5H_4NAlMe_3$) **Int5a** (Scheme 1 and Figure 4). In **TS4a**, the C^6–C^8 distance considerably decreases, while the Ni–C^6 (1.935 Å) and the Ni–C^8 (2.006 Å) distances marginally change from those in **Int4a**. These geometry changes suggest that the C^6–C^8 bond formation is in progress in **TS4a** with keeping the Ni–C^6 and Ni–C^8 bonds. The $\Delta G^{\circ\ddagger}$ value (2.1 kcal mol^{-1}) is small, indicating that the C^6–C^8 bond formation occurs easily to afford nickel(0) butadienyl pyridyl complex **Int5a**, which is much more stable than **Int4a** by 25.1 kcal mol^{-1}. In **Int5a**, the C^6–C^8 bond (1.340 Å) is completely formed. This **Int5a** is essentially the same as **Int3a** with only one difference, that **Int5a** has one butadienyl group but **Int3a** has one vinyl group. Thus, **Int5a** undergoes one more acetylene coordination, which is named as the third acetylene coordination hereafter, to afford nickel(II) butadienyl pyridyl acetylene intermediate Ni(NHC)(C_4H_5)-($C_5H_4NAlMe_3$)(C_2H_2) **Int6a**. This coordination occurs with considerably large stabilization energy of −12.6 kcal mol^{-1}. The next step is the C^4–C^7 bond formation by the reductive elimination, which occurs via a transition state **TS5a** ($\Delta G^{\circ\ddagger}$ = 4.2 kcal mol^{-1}) to afford a para-substituted butadienyl-pyridine–$AlMe_3$ **P2a** with the regeneration of active species **1**.[36] The rate-determining step is the C^4–H bond activation in this catalytic cycle, too. The Gibbs reaction energy for the formation of **P2a** is −72.5 kcal mol^{-1}. These computational results leads to the conclusion that **P2a** is a major product because the $\Delta G^{\circ\ddagger}$ value for the C^6–C^8 bond formation via alkyne insertion is smaller than that of the C^4–C^6 bond formation via reductive elimination of **P1a**. This conclusion is not consistent with the experimental fact that **P1a** is a major product. We will explain below the reason for this discrepancy and explain the conditions necessary for the formation of **P1a**.

Geometry and Energy Changes in the C^2- and C^3-Alkenylation of Pyridine with Ni(NHC)/$AlMe_3$ Catalyst. The C^2- and C^3-alkenylations occur in a similar manner to that of the C^4-alkenylation; Figures S1 to S6 show geometry and energy changes. Hence, important differences from those of the C^4-alkenylation are discussed here; the labels **a**, **b**, and **c** will be used for the C^4-, C^3-, and C^2-alkenylations, respectively, to avoid confusion. The oxidative addition of the C–H bond is the rate-determining step in all three alkenylations (Figures S3 and S6). The transition states **TS2b** and **TS2c** are similar to **TS2a**, where the H^1 atom directly migrates from pyridine to acetylene. The $\Delta G^{\circ\ddagger}$ value (22.0 kcal mol^{-1}) for the C^2–H bond activation is much larger than those of the C^3–H (21.5 kcal mol^{-1}) and C^4–H bond (17.4 kcal mol^{-1}) activations, indicating that the C^2-substituted pyridine is not produced well and the C^3-substituted pyridine is less produced than the C^4 one. The reasons will be discussed below. After the C–H bond activation, two kinds of C–C bond formation are possible; one is the C^2–C^6 and C^3–C^6 bond formations via the reductive elimination to afford vinyl-substituted pyridine–$AlMe_3$ **P1**. Another is the second acetylene insertion into the Ni–vinyl bond (C^6–C^8 bond formation) followed by the C^2–C^7, C^3–C^7, and C^4–C^7 bond formations via

DOI: 10.1021/acs.joc.6b02394
J. Org. Chem. 2017, 82, 289–301

Table 1. Gibbs Energy Changes ($\Delta G°$ in kcal mol^{-1})[a] for Oxidative Addition of C^n−H (n = 2, 3, and 4) Bond, the C^n−C^6 and C^6−C^8 Bond Formations, and the Second Acetylene Coordination in the Ni(NHC)/AlMe$_3$-Catalyzed Reaction

	Gibbs energy $\Delta G°$						
C^n-alkenylation	C^n−H bond activation	2nd acetylene coordination[b]	reductive elimination of **P1**	acetylene insertion into Ni−vinyl bond	3rd acetylene coordination[c]	reductive elimination of **P2**	$\Delta G°$ **P1** (**P2**)
				Acetylene, HC≡CH			
C^4-alkenylation	17.4	−12.7	4.8	2.1	−12.6	4.2	−33.5 (−72.5)
C^3-alkenylation	21.5	−9.9	7.9	3.4	−14.8	5.9	−34.9 (−69.6)
C^2-alkenylation	22.0	−6.2	4.5	3.4	−4.6	2.4	−31.7 (−86.5)
				1,2-Dimethyl Acetylene, MeC≡CMe			
C^4-alkenylation	16.7	−5.1	6.8	5.3	8.4	6.2	−24.2 (−43.8)
C^3-alkenylation	17.9	−4.4	8.0	3.7	8.3	10.4	−22.7 (−43.2)
C^2-alkenylation	21.5	−2.5	11.4	3.3	7.0	18.3	−19.3 (−39.9)
				1,2-Diisopropyl Acetylene, ^{i}PrC≡C^{i}Pr			
C^4-alkenylation	17.6	−3.0	7.0	9.5	21.1	–[d]	−23.4 (−34.9)
C^3-alkenylation	19.0	−3.9	4.3	8.2	23.0	–[d]	−22.3 (−35.2)
C^2-alkenylation	22.5	9.1	10.3	8.3	16.7	–[d]	−16.5 (−31.6)

[a]The B3LYP-D3/BS-II method was employed. [b]The second acetylene coordination with **Int3** leads to the formation of **Int4**. See Scheme 1 for details. [c]The third acetylene coordination with **Int5** leads to the formation of **Int6**. See Scheme 1 for details. [d]No reaction occurs.

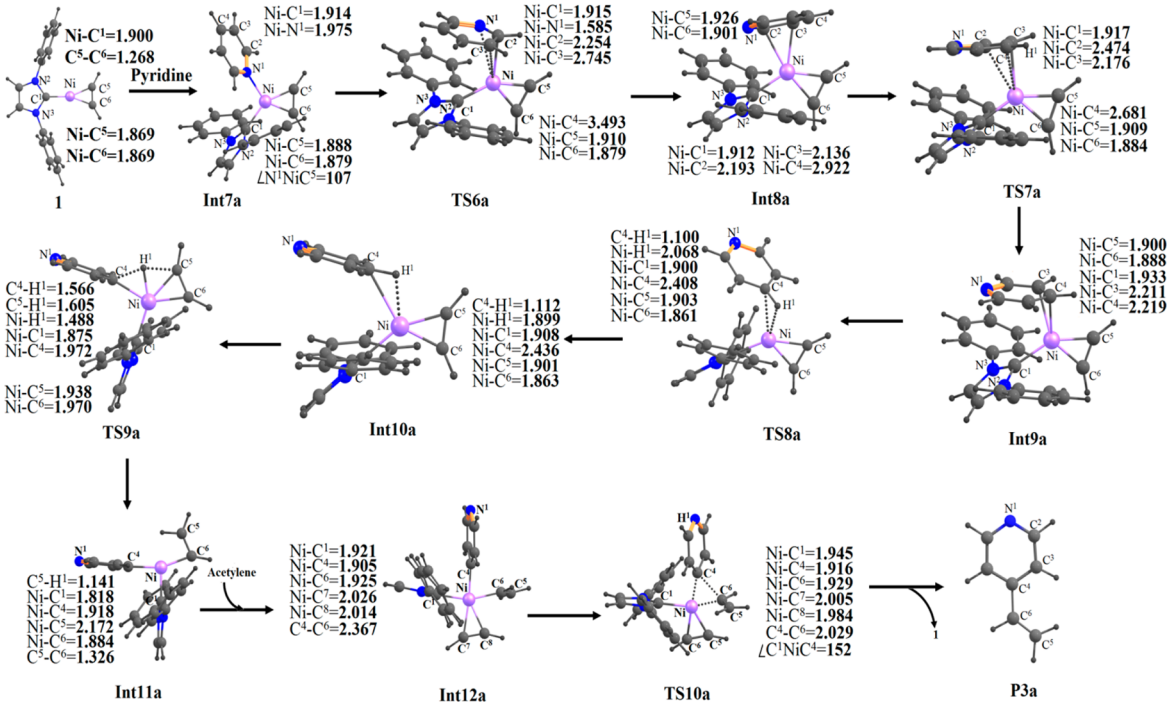

Figure 5. Geometrical changes in the C^4-alkenylation of pyridine by the Ni(NHC) catalyst in the absence of AlMe$_3$, leading to the formation of vinyl pyridine **P3a**. Distances are given in angstroms, and angles are in degrees.

reductive elimination to afford butadienyl-substituted pyridine−AlMe$_3$ **P2**. Both of these C−C bond formation reactions occur easily with small $\Delta G°^{‡}$ value (Table 1). Based on these results, it is concluded that the C^4-alkenylation occurs more easily than the C^3-alkenylation, which is consistent with the experimental report that the C^4-substituted pyridine−AlMe$_3$ is a major (53% yield) product, the C^3-substituted pyridine−AlMe$_3$ is a minor (15% yield) product, and the C^2-substituted pyridine−AlMe$_3$ is not produced.

Substituent Effects of Acetylene on the C^n-Alkenylation (n = 2, 3, and 4) of Pyridine with Ni(NHC)/AlMe$_3$ Catalyst. We investigated here the reactions of dimethylacetylene and diisopropylacetylene to elucidate the substituent effects of acetylene moiety on the alkenylation reaction. As seen in Table 1, the $\Delta G°^{‡}$ value for the oxidative addition of the C−H bond (**TS2**) is similar between the substituted and nonsubstituted acetylenes, as expected. The $\Delta G°^{‡}$ values for **TS3** (the reductive elimination of **P1** via the C^4−C^6 bond formation.) and **TS4** (the second acetylene insertion into the Ni−vinyl bond via the C^6−C^8 bond formation) increase in the order acetylene < dimethyl acetylene ≪ diisopropyl acetylene (Table 1). In the C^2-alkenylation, these $\Delta G°^{‡}$ values increase more than the C^3 and C^4 ones. One more important result in the real substrate (1,2-diisopropylacetylene) is that, in C^4-alkenylation, the $\Delta G°^{‡}$ value for the second acetylene insertion into the Ni−vinyl bond (**TS4**) becomes larger than that of the reductive elimination (**TS3**) of vinyl pyridine **P1**, indicating that, in the case of the real substrate, butadienyl-pyridine−AlMe$_3$ **P2a** cannot be produced but vinyl pyridine−AlMe$_3$ **P1a** is produced. These computational results

DOI: 10.1021/acs.joc.6b02394
J. Org. Chem. 2017, 82, 289−301

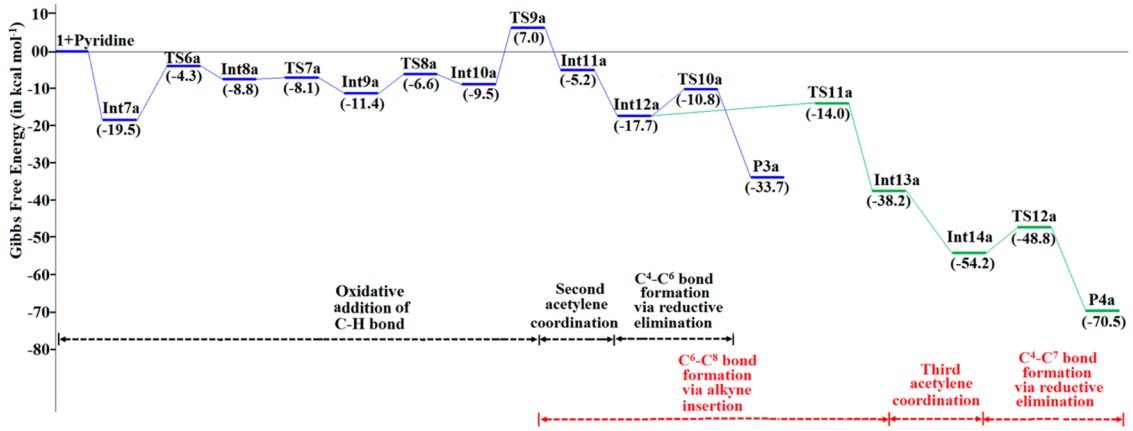

Figure 6. Gibbs energy changes (kcal mol^{-1}) in the C^4-alkenylation of pyridine by the Ni(NHC) catalyst in the absence of $AlMe_3$. The B3LYP-D3/BS-II method was used.

Table 2. Gibbs Energy Changes ($\Delta G°$ in kcal mol^{-1})[a] for Oxidative Addition of C^n−H (n = 2, 3, and 4) Bond, the C^n−C^6 and C^6−C^8 Bond Formations, and the Second Acetylene Coordination in the Ni(NHC)-Catalyzed Reaction without $AlMe_3$

	Gibbs Energy $\Delta G°$						
C^n-alkenylation	C^n-H bond activation	2nd acetylene coordination	reductive elimination of P3	acetylene insertion into Ni−vinyl bond	3rd acetylene coordination	reductive elimination of P4	$\Delta G°$ **P3** (**P4**)
				Acetylene, HC≡CH			
C^4-alkenylation	26.5	−12.5	6.9	3.7	−16.0	5.4	−33.7 (−70.5)
C^3-alkenylation	28.2	−8.6	6.1	3.1	−10.0	5.6	−33.1 (−69.9)
C^2-alkenylation	27.7	−10.5	4.8	2.8	−3.8	1.3	−34.0 (−70.7)
				1,2-Diisopropyl Acetylene, ^{i}PrC≡C^{i}Pr			
C^4-alkenylation	26.3	1.2	4.5	4.4	6.4	15.4	−21.0 (−32.9)
C^3-alkenylation	26.6	1.2	10.1	7.1	14.4	9.8	−20.2 (−32.3)
C^2-alkenylation	27.1	−2.0	5.1	9.6	7.0	11.4	−21.7 (−32.6)

[a]The B3LYP-D3/BS-II method was employed.

of the real substrates agree with the experimental ones that the C^4-substituted vinyl pyridine product **P1a** is a major product.

Catalytic Cycle for C^n-Alkenylation (n = 2, 3, and 4) of Pyridine with Ni(NHC) Catalyst in the Absence of $AlMe_3$: Geometry and Energy Changes. The C^4-alkenylation of pyridine in the absence of $AlMe_3$ occurs with geometrical changes shown by Figures 5 and S7. The first step is pyridine coordination with the Ni atom through the N atom, leading to the formation of nickel(0) pyridine acetylene intermediate Ni(NHC)(C_5H_5N)(C_2H_2) **Int7a**. This intermediate is substantially more stable than **1** by −19.5 kcal mol^{-1}, as shown in Figure 6. **Int7a** isomerizes to a less stable intermediate **Int10a** through several intermediates and transition states, where **Int7a**, **Int8a**, and **Int9a** correspond to rotational isomers of pyridine around the Ni−N bond. In **Int10a**, the C^4−H bond is moderately elongated to 1.112 Å and the Ni−H distance is rather short (1.899 Å), suggesting that **Int10a** is an intermediate leading to the C^4−H bond activation. The C^4−H bond activation occurs through a transition state **TS9a** to afford an intermediate **Int11a**. The geometry of **TS9a** (Figure 5) is similar to that of **TS2a** (Figure 2), while the Ni−H distance (1.488 Å) is slightly longer and the C^4−H (1.566 Å) and C^5−H (1.605 Å) distances are considerably shorter in **TS9a** than in **TS2a**. These geometrical features suggest that **TS9a** is more congested than **TS2a**. The $\Delta G°^{\ddagger}$ value is 26.5 kcal mol^{-1} relative to **Int7a** and 16.5 kcal mol^{-1} relative to **Int10a**; see Figure 6 and Table 2. It should be noted that these $\Delta G°^{\ddagger}$ values are larger than those in the presence of $AlMe_3$ (Figure 3), the reason for which will be discussed below. The next step is C^4−C^6, C^6−C^8, or C^4−C^7 bond formation which occurs in a similar manner to those in the presence of $AlMe_3$. The $\Delta G°^{\ddagger}$ value of this step is small, indicating that this step occurs easily.

The C^3- and C^2-alkenylations in the absence of $AlMe_3$ occur similarly to the C^4-alkenylation; see Figures S8 to S10 and Figures S11 to S13 for the C^3- and C^2-alkenylations, respectively. The pyridine rotation around the Ni−N bond occurs one time in the C^3-alkenylation to afford **Int10b** through **Int8b**. In the C^2-alkenylation, **Int7c** is directly converted to **Int10c** without pyridine rotation. After **Int10b** and **Int10c**, the C^3- and C^2-alkenylations occur with similar $\Delta G°^{\ddagger}$ values to that of the C^4-alkenylation. Because the $\Delta G°^{\ddagger}$ values of all these three C−H bond activations are considerably larger than those of the C^4−C^6, C^6−C^8, and the C^4−C^7 bond formations, as shown in Table 2, the C−H bond activation is rate-determining. As mentioned above, these $\Delta G°^{\ddagger}$ values are considerably larger than those in the presence of $AlMe_3$ (Table 1).

This result leads to a clear explanation of the reason why $AlMe_3$ equimolar to Ni(0) (i.e., much less than substrate) is enough for the C^4-alkenylation, as follows: Because $AlMe_3$ concentration is much less than the pyridine one, both pyridine and pyridine−$AlMe_3$ adduct are involved in the catalytic reaction. Pyridine more strongly coordinates with Ni(NHC), but the C−H bond activation needs a much larger $\Delta G°^{\ddagger}$ value. This means that pyridine forms a more stable adduct Ni(NHC)(pyridine)(acetylene) but it is not reactive. On the other hand, the concentration of pyridine−$AlMe_3$ adduct is small but its adduct with Ni(NHC) is reactive. Important is the energy of the highest transition state in the catalytic cycle. In the absence of $AlMe_3$,

DOI: 10.1021/acs.joc.6b02394
J. Org. Chem. 2017, 82, 289−301

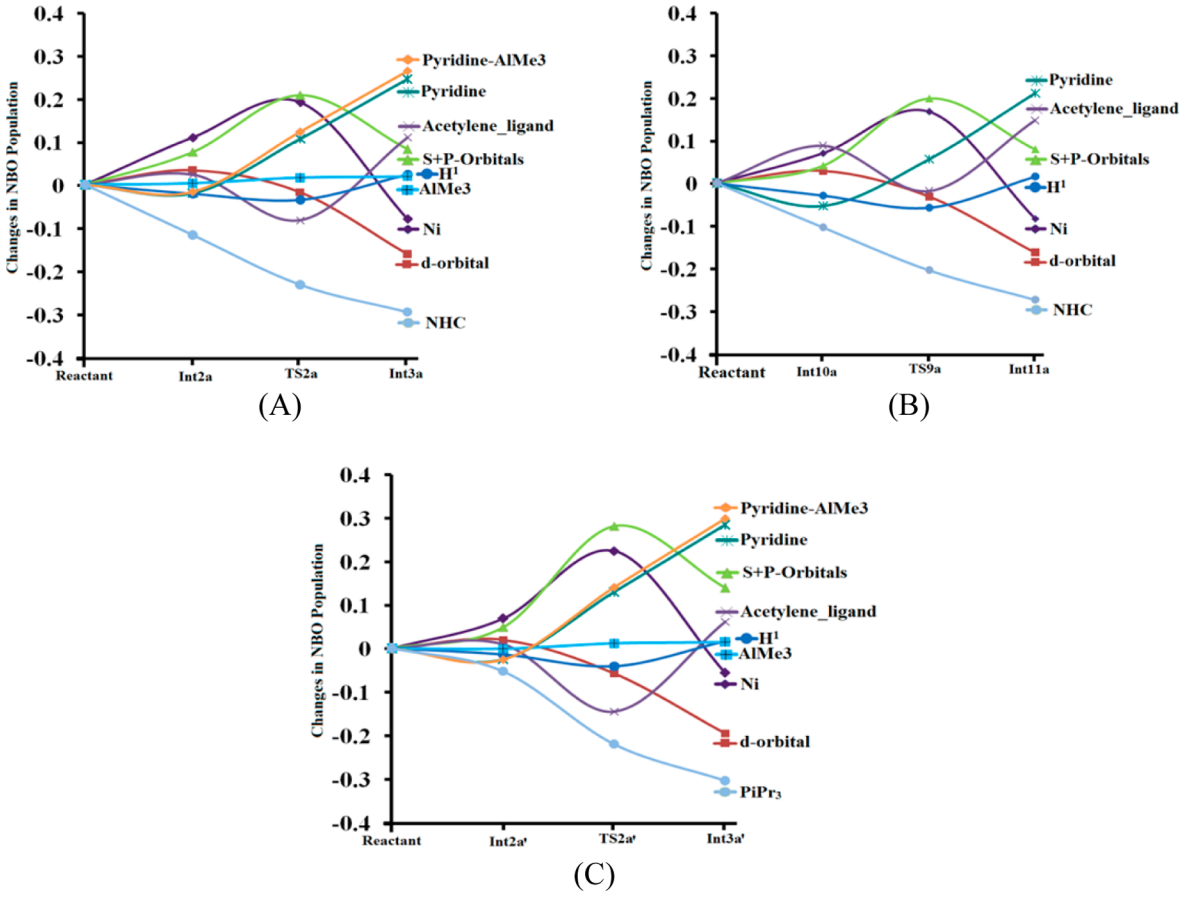

Figure 7. Changes in the NBO population in the oxidative addition of the C^4−H bond by (A) Ni(NHC)/$AlMe_3$ and (B) Ni(NHC) in the absence of $AlMe_3$, and (C) Ni(P(*i*-Pr)$_3$)/$AlMe_3$ catalyst. The B3LYP/BS-II method was used.

Scheme 2. Exchange Repulsion between the σ_{C-H} Bonding (or Antibonding) Orbitals of Pyridine and π Orbital of Acetylene

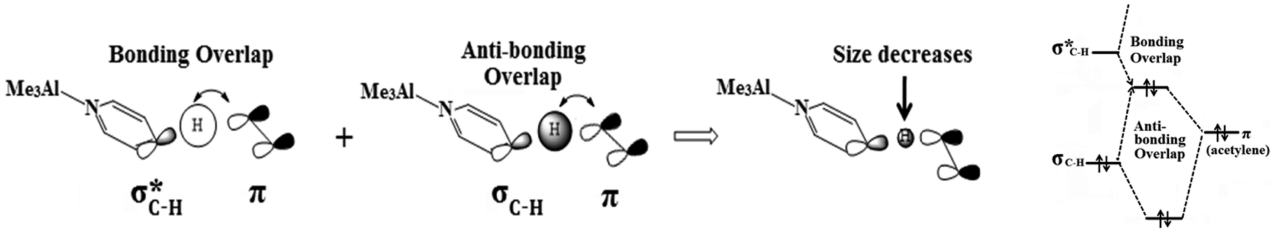

TS9a is the highest energy transition state (7.0 kcal mol^{-1}; see Figure 6), whereas in the presence of $AlMe_3$, **TS2a** is the highest energy transition state (1.6 kcal mol^{-1}; see Figure 3). These results clearly indicate that the reaction via **TS2a** much easily occurs than that via **TS9a**.

We will briefly discuss here the reaction of substituted acetylene in the absence of $AlMe_3$ (Table 2). The C−H bond activation is influenced little by the substituents of acetylene, as expected. The $\Delta G^{\circ\ddagger}$ values for other steps are small. These results indicate that the alkenylation reactions with the real acetylene are difficult in the absence of $AlMe_3$, too.

Electronic Processes in C^n-Alkenylation (n = 2, 3, and 4) of Pyridine with and without $AlMe_3$. To understand the electronic process, we investigated changes in NBO population by the C−H bond activation, because it is a rate-determining step. When going from reactants to **TS2a**, the electron population of the NHC ligand substantially decreases and that of acetylene moderately increases at **Int2a** but then somewhat decreases, as shown in Figure 7A. On the other hand, the electron populations of Ni and pyridine considerably increase. The increase in the Ni atomic population mainly arises from the increases in the s and p orbital populations, while the d orbital population moderately decreases. These population changes lead to the following understanding of electronic processes: The electron population of acetylene increases in **Int2a** by the π-back-donation from Ni to acetylene, but the π-back-donation becomes weaker as going from **Int2a** to **TS2a**. Though this weakening of π-back-donation should increase the Ni d orbital population, the d orbital population decreases because charge transfer (CT) occurs from the Ni d orbital to pyridine, as often found in the usual oxidative addition reaction.[34,37] Actually, the electron population of pyridine increases in **TS2a**, as was seen above. However, the H atomic population changes little unexpectedly, when going from **Int2a** to **TS2a**, unlike in the concerted oxidative addition.[34,37] This unexpected result in the H atomic population is one of the characteristic features of this C−H

DOI: 10.1021/acs.joc.6b02394
J. Org. Chem. 2017, 82, 289−301

Scheme 3. ONIOM Procedure for the Evaluation of Steric Repulsion

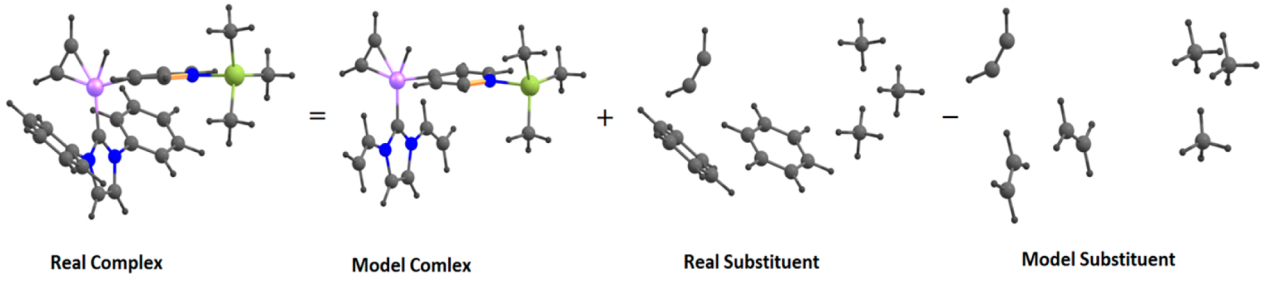

activation reaction: The CT from Ni d MO to the C−H σ^* MO is necessary to induce the C−H bond weakening which increases in the H atomic population. However, the exchange repulsion of the C−H σ MO with the π MO of acetylene is simultaneously induced because the H atom is approaching the acetylene. Because the phase of H 1s orbital is different between the bonding and antibonding overlaps, the H atomic population decreases in **TS2a**, as schematically shown in Scheme 2. This exchange repulsion does not occur in the usual concerted oxidative additions.

As going from **TS2a** to **Int3a**, the electron population of the NHC further decreases. Also, the Ni atomic population starts to decrease substantially, in which all s, p, and d orbital populations decrease. On the other hand, the electron populations of the acetylene and pyridine moieties considerably increase. These population changes suggest that the acetylene and pyridine moieties are converted to an anionic vinyl group and an anionic pyridyl group, respectively, which are consistent with the understanding that this is the oxidative addition of the C−H bond to the Ni−acetylene moiety.[34] In the C^2- and C^3-alkenylation reactions, essentially the same population changes are observed; see Figures S14A and S15A and Tables S1 to S3.

In the C^4-alkenylation by Ni(NHC) in the absence of $AlMe_3$, the NBO population changes occur in a different manner from those by Ni(NHC)/$AlMe_3$, as compared in Figures 7A and 7B. In **TS2a**, the electron population of the pyridine−$AlMe_3$ moiety more increases (0.107*e*) than in **TS9a** (0.056*e*) without $AlMe_3$. This result suggests that the CT from the Ni d orbital to pyridine occurs more in the presence of $AlMe_3$ than in the absence of $AlMe_3$. Because $AlMe_3$ is a Lewis acid, it stabilizes the π^* MO of pyridine to enhance the CT from Ni(NHC). This is one reason why the C−H bond activation occurs with smaller $\Delta G^{\circ\ddagger}$ value by the presence of $AlMe_3$. The population changes when going from **TS9a** to **Int11a** occur in a similar manner to those in the reaction with $AlMe_3$, indicating that $AlMe_3$ influences only the C−H bond activation. In the C^2- and C^3-alkenylation reactions without $AlMe_3$, the population changes occur in essentially the same manner as those in the C^4-alkenylation reaction without $AlMe_3$; see Figures S14B and S15B and Tables S4−S6, respectively. We will skip the discussion of these reactions.

Selectivity of the C^4- and C^3-Alkenylations over the C^2-Alkenylation of Pyridine by Ni(NHC)/$AlMe_3$ Catalyst. In order to find the reason for selectivity of the C^4- and C^3-alkenylations over the C^2-alkenylation of pyridine by the Ni(NHC)/$AlMe_3$ catalyst, we inspected two factors: (i) the steric repulsion between $AlMe_3$ and *N*,*N*-diphenyl NHC ligand and (ii) the CT interaction in the transition state of the C−H bond activation.

For the evaluation of the steric repulsion, we employed the ONIOM procedure (Scheme 3). The total energy of the real system is approximately represented by eq 1.

$$E_{RC} = E_{MC} + E_{RS} - E_{MS} \quad (1)$$

where subscripts RC, MC, RS, and MS represent a real complex, a model complex, real substituents, and model substituents, respectively (Scheme 3). To check the reliability of eq 1, we calculated the activation barrier ($\Delta E^{\ddagger}$) of the C−H bond activation, where only electronic energy was considered.[38] The $\Delta E^{\ddagger}$ value is represented by eq 2. The calculated value agrees with that of the real system in all three alkenylations (Table 3), suggesting that this procedure is useful for making analysis.

Table 3. Activation Energies $\Delta E^{\ddagger}$[a] (in kcal mol^{-1}) Calculated for Real Complex and Model Complex and the Steric Repulsion $\Delta E^{\ddagger}_{SR}$ (in kcal mol^{-1}) in the Transition State of the C^n−H (n = 2, 3, and 4) Bond Activation Calculated at the B3LYP-D3 Level

	$\Delta E^{\ddagger}$			
C^n-alkenylation	real complex	model complex	ONIOM	$\Delta E^{\ddagger}_{SR}$
	N,*N*-Diphenyl NHC Ligand[b]			
C^4-alkenylation	23.62	22.89	24.55	1.66
C^3-alkenylation	23.91	23.77	25.64	1.86
C^2-alkenylation	24.16	21.49	26.84	5.35
	P(*i*-Pr)$_3$ Ligand[c]			
C^4-alkenylation	18.71	20.13	22.20	2.07
C^3-alkenylation	19.82	21.00	23.01	2.02
C^2-alkenylation	16.05	15.89	17.27	1.38

[a]The electronic energies were considered. See ref 38 for details. [b]See Scheme 3. [c]See Scheme S1.

$$\Delta E^{\ddagger} = E_{RC\ at\ TS2} - E_{RC\ at\ Int1} = \Delta E^{\ddagger}_{MC} + \Delta E_{RS} - \Delta E_{MS} \quad (2)$$

$$\Delta E^{\ddagger}_{MC} = E_{MC\ at\ TS2} - E_{MC\ at\ Int1} \quad (3a)$$

$$\Delta E^{\ddagger}_{SR} = \Delta E_{RS} - \Delta E_{MS} = (E_{RS} - E_{MS})_{at\ TS2} - (E_{RS} - E_{MS})_{Int1} \quad (3b)$$

The $\Delta E^{\ddagger}_{MC}$ (eq 3a) corresponds to the activation energy of the model system without bulky substituent. The difference in the $\Delta E^{\ddagger}_{MC}$ between the presence and absence of $AlMe_3$ represents the electronic effect of $AlMe_3$; see Table S7. The difference between the real (ΔE_{RS}) and model substituents (ΔE_{MS}) corresponds to the effect of steric repulsion ($\Delta E^{\ddagger}_{SR}$ in eq 3b). In the real complex, the $\Delta E^{\ddagger}$ value in the C^4-alkenylation is smaller than those in the C^3- and C^2-alkenylations by 0.29 kcal mol^{-1} and 0.54 kcal mol^{-1}, respectively (Table 3). In the model complex, the $\Delta E^{\ddagger}_{MC}$ value in the C^4-alkenylation is smaller than in the C^3-alkenylation by 0.88 kcal mol^{-1} but larger than in the C^2-alkenylations by 1.40 kcal

DOI: 10.1021/acs.joc.6b02394
J. Org. Chem. 2017, 82, 289−301

Table 4. Gibbs Energy Changes ($\Delta G°$ in kcal mol^{-1})[a] for Oxidative Addition of C^n−H (n = 2, 3, and 4) Bond, the C^n−C^6 and C^6−C^8 Bond Formations, and the Second Acetylene Coordination in the Ni(P(i-Pr)$_3$)/AlMe$_3$-Catalyzed Reaction

	Gibbs energy $\Delta G°$						
C^n-alkenylation	C^n-H bond activation	2nd acetylene coordination[b]	reductive elimination of **P1′**	acetylene insertion into Ni−vinyl bond	3rd acetylene coordination[c]	eductive elimination of **P2′**	$\Delta G°$ **P1′** (**P2′**)
				Acetylene, HC≡CH			
C^4-alkenylation	13.0	3.1	3.1	4.1	−3.3	3.4	−33.5 (−72.5)
C^3-alkenylation	14.8	−1.0	5.2	4.1	−0.7	4.3	−34.9 (−69.6)
C^2-alkenylation	12.6	−2.4	7.0	4.8	−7.5	10.2	−31.7 (−86.5)
				1,2-Dimethyl Acetylene, MeC≡CMe			
C^4-alkenylation	14.4	0.4	2.7	13.9	−8.6	8.7	−24.2 (−43.8)
C^3-alkenylation	15.4	−1.0	7.8	12.7	−6.4	11.1	−22.7 (−43.2)
C^2-alkenylation	13.3	0.7	9.8	5.9	−1.1	10.6	−19.3 (−39.9)
				1,2-Diisopropyl Acetylene, ^{i}PrC≡C^{i}Pr			
C^4-alkenylation	14.1	3.4	9.3	6.7	2.4	9.9	−23.4 (−34.9)
C^3-alkenylation	15.2	2.4	4.9	9.1	−0.4	12.5	−22.4 (−35.2)
C^2-alkenylation	14.8[d]	3.9	14.1	12.2	9.5[e]	13.3	−16.5 (−31.6)

[a]The B3LYP-D3/BS-II method was employed. [b]The second acetylene coordination with **Int3′** leads to the formation of **Int4′**. See Scheme 1 for details. [c]The third acetylene coordination with **Int5′** leads to the formation of **Int6′**. See Scheme 1 for details. [d]See Tables S10 and discussion on page S37 of the Supporting Information. [e]See Table S11 on page S38 of the Supporting Information.

mol^{-1}, indicating that the electronic factor is not responsible for the small C^2-selectivity. On the other hand, the $\Delta E^{\ddagger}_{SR}$ is very large in the C^2-alkenylation and decreases in the order C^2- ≫ C^3- > C^4-alkenylation, indicating that the steric repulsion between the *N*,*N*-diphenyl NHC ligand and AlMe$_3$ is the largest in the C^2-alkenylation and becomes small in both the C^3- and C^4-alkenylations. In other words, AlMe$_3$ induces large steric repulsion with *N*,*N*-diphenyl NHC ligand in the C^2-alkenylation. This steric repulsion mainly determines the regioselectivity of C^2-, C^3-, and C^4-alkenylations.

We investigated here the electronic factor in more detail. In **TS2**, the electron population of the pyridine−AlMe$_3$ moiety decreases in the order C^2- (0.131*e*) ≥ C^4- (0.124*e*) ≫ C^3-alkenylation (0.095*e*), where in parentheses is the increase in the population going from **Int2a** to **TS2a**. On the other hand, the Ni d orbital population decreases more in the C^2- (−0.033*e*) than in the C^3-alkenylation (−0.026*e*), and it decreases the least in the C^4-alkenylation (−0.017*e*); see Tables S1 to S3. These population changes in pyridine−AlMe$_3$ and Ni d orbital suggest that the CT (ML → pyridine−AlMe$_3$) is substantially larger in the C^2- and C^4-alkenylations than in the C^3-alkenylation. The larger CT interaction stabilizes **TS2** of the C^2- and C^4-alkenylations compared to that of the C^3-alkenylation. These results indicate that the electronic effect is favorable for the C^2- and C^4-alkenylations; in other words, the selectivity of the C^4-alkenylation over the C^3-alkenylation arises from the electronic effect.

In summary, it is concluded that both electronic and steric factors contribute to the larger C^4-selectivity over the C^3 and C^2 ones in pyridine alkenylation by the Ni(NHC)/AlMe$_3$ catalyst.

Reasons Why AlMe$_3$ Accelerates Alkenylation of Pyridine. As discussed above, the important difference between the alkenylation reaction with and without AlMe$_3$ arises from the difference in the initial intermediate complex. In the absence of AlMe$_3$, the N atom of pyridine coordinates with the Ni atom to form **Int7** in the first step. This coordination is not possible in the presence of AlMe$_3$ because AlMe$_3$ strongly interacts with pyridine through the N atom. Thus, the C−C bond of pyridine−AlMe$_3$ coordinates with Ni atom in an η^2-fashion to form **Int1**. **Int7** is more stable than **Int1** by 4 kcal mol^{-1} (Figures 3 and 6). The stabilization of **Int7** increases the Gibbs activation energy. This is one of the reasons why the alkenylation reaction is difficult in the absence of AlMe$_3$.

Another reason is found in the CT interaction at the transition state of the C−H bond activation. As going from **Int2** to **TS2**, the electron population of the pyridine moiety increases (by 0.130*e* in the C^2-, 0.083*e* in the C^3-, and 0.107*e* in the C^4-alkenylations) more in **TS2** with AlMe$_3$ than in **TS9** without AlMe$_3$ (0.057*e* in the C^2-, 0.044*e* in the C^3-, and 0.056*e*, in the C^4-alkenylations). These results indicate that the CT(Ni(NHC) → pyridine−AlMe$_3$) is larger than the CT(Ni(NHC) → pyridine). This enhancement of the CT interaction by AlMe$_3$ more stabilizes **TS2** than **TS9**. It is noted that the enhancement of CT interaction is the largest in the C^4-alkenylation but the least in the C^3 one. Based on these results, another important reason is the enhancement of CT by AlMe$_3$. This is not surprising because CT occurs from pyridine to AlMe$_3$ to stabilize the π^* orbital and to enhance the CT from the Ni to pyridine.

Effects of Triisopropylphosphine P(i-Pr)$_3$ on Reactivity and Regioselectivity of the C^n-Alkenylation in the Presence of AlMe$_3$. In another experimental work by Hiyama and Nakao,[15] the C^2-alkenylation succeeded by employing Ni(P(i-Pr)$_3$) with either AlMe$_3$ or ZnMe$_2$ as LA. In this reaction, vinyl- and butadienyl-pyridine were produced selectively by employing appropriate Lewis acid; for instance, when Ni(P(i-Pr)$_3$)/AlMe$_3$ was employed, C^2-substituted butadienyl pyridine was produced as a major product unlike in the Ni(NHC)/AlMe$_3$-catalyzed reaction. It is interesting to explore the reasons why the C^2-butadienyl pyridine is produced as a main product when Ni(P(i-Pr)$_3$)/AlMe$_3$ catalyst is employed, because such product is not produced in the reaction by the Ni(NHC)/AlMe$_3$ catalyst. The geometry and energy changes for the C^4-alkenylations are shown in Figures S16 to S18, and those for the C^3- and C^2-alkenylations are in Figures S19 to S24. These geometry changes are similar to those by the Ni(NHC)/AlMe$_3$ catalyst, and hence the discussion of the geometry changes is skipped here. As seen in Table 4, the $\Delta G^{\circ\ddagger}$ values for the C−H bond activation by the Ni(P(i-Pr)$_3$)/AlMe$_3$ catalyst are much smaller in all three alkenylations than those by the Ni(NHC)/AlMe$_3$ catalyst, though the $\Delta G^{\circ\ddagger}$ values for the second acetylene insertion and

DOI: 10.1021/acs.joc.6b02394
J. Org. Chem. 2017, 82, 289−301

the C−C bond reductive elimination are similar to or marginally larger than those by the Ni(NHC)/$AlMe_3$ catalyst. Because these $\Delta G^{\circ\ddagger}$ values are smaller than that of the C−H bond activation, the C−H bond activation is rate-determining. Therefore, it is concluded that the alkenylation of pyridine occurs much more easily when P(*i*-Pr)$_3$ ligand was employed instead of *N*,*N*-diphenyl-NHC ligand.

One important result in Table 4 is that the $\Delta G^{\circ\ddagger}$ value is the smallest in the C^2-alkenylation (12.6 kcal mol^{-1}) by the Ni(P(*i*-Pr)$_3$)/$AlMe_3$ catalyst indicating that the C^2-alkenylation occurs more favorably than the C^3- and C^4-alkenylations, when the Ni(P(*i*-Pr)$_3$)/$AlMe_3$ catalyst was used. These results agree with the experimental fact that the C^2-alkenylation occurs by the Ni(P(*i*-Pr)$_3$)/$AlMe_3$ catalyst. Another important difference is that the butadienyl pyridine is produced as a main product. To yield such product, the second acetylene coordinates easily with **Int3a′** to afford **Int4a′**. After **Int4a′**, the acetylene insertion (**TS4′**) into the Ni−vinyl bond must more easily occur than the C−C reductive elimination (**TS3′**) of the vinyl group. As seen in Table 4, the $\Delta G^{\circ\ddagger}$ value for the reductive elimination of vinyl group is larger than that of the acetylene insertion into the Ni−vinyl bond in the C^2-alkenylation for both unsubstituted and substituted acetylenes. Therefore, the C^2-butadienyl pyridine is mainly produced. These results are also consistent with the experimental results that the C^2-substituted butadienyl pyridine is a main product.

Reasons Why C^2-Alkenylation by Ni(P(*i*-Pr)$_3$)/$AlMe_3$ Catalyst Occurs but It Is Difficult with Ni(NHC)/$AlMe_3$ Catalyst. As discussed above, the $\Delta G^{\circ\ddagger}$ value for the C−H bond activation (12 to 16 kcal mol^{-1}) is smaller in the alkenylation reactions by the Ni(P(*i*-Pr)$_3$)/$AlMe_3$ catalyst than that by the Ni(NHC)/$AlMe_3$ catalyst (17 to 22 kcal mol^{-1}); especially the $\Delta G^{\circ\ddagger}$ value for the C^2−H bond activation is much smaller (12.6 kcal mol^{-1}) in the NiP(*i*-Pr)$_3$/$AlMe_3$-catalyzed reaction than in the Ni(NHC)/$AlMe_3$-catalyzed reaction (22 kcal mol^{-1}). To inspect the reason for these results, we investigated the steric repulsion of $AlMe_3$ with NHC and P(*i*-Pr)$_3$ ligands. To evaluate the steric repulsion, the ONIOM scheme shown in Scheme S1 and eq 1 was employed, as discussed above. As seen in Table 3, the steric repulsion (2.07 kcal mol^{-1}) in the C^4-alkenylation is somewhat larger in the NiP(*i*-Pr)$_3$/$AlMe_3$ catalyst than in the Ni(NHC)/$AlMe_3$ catalyst (1.66 kcal mol^{-1}). In the C^3-alkenylation, the steric repulsion in the NiP(*i*-Pr)$_3$/$AlMe_3$ catalyst is moderately larger (2.02 kcal mol^{-1}) than in the Ni(NHC)/$AlMe_3$ catalyst (1.86 kcal mol^{-1}). On the other hand, the steric repulsion in the C^2-alkenylation (1.38 kcal mol^{-1}) is substantially smaller in the NiP(*i*-Pr)$_3$/$AlMe_3$ catalyst than in the Ni(NHC)/$AlMe_3$ one (5.37 kcal mol^{-1}). These results suggest that the smaller steric repulsion favors the C^2-alkenylation by the Ni(P(*i*-Pr)$_3$)/$AlMe_3$ catalyst over the Ni(NHC)/$AlMe_3$ catalyst. The steric repulsion reflects in the C^n-Ni-NHC and C^n−Ni-P angles (C^n = the pyridine C atom reacting with H atom) in **TS2** of the Ni(NHC)/$AlMe_3$ and Ni(P(*i*-Pr)$_3$)/$AlMe_3$ reaction systems, respectively, because it is likely that the large steric repulsion increases these angles. We examined the relation between the steric repulsion and these angles and found that, in the Ni(NHC)/$AlMe_3$ catalyst, the C^2−Ni−NHC angle is larger in the C^2-alkenylation than the corresponding angles in the C^3- and C^4-alkenylations but, in the Ni(P(i-Pr)$_3$)/$AlMe_3$ catalyst, the C^2−Ni−P angle is smaller in the C^2-aklenylation than in the others. These results indicate again that the steric repulsion plays an important role in determining the regioselectivity and also that the difference in regioselectivity between the Ni(NHC)/$AlMe_3$ and Ni(P(i-Pr)$_3$)/$AlMe_3$ catalysts arises from the difference in steric repulsion; see the discussion on page S39 and Table S12.

The electronic effect is also important for accelerating the C^2−H bond activation over the C^3−H and C^4−H bond activations. The population changes in the alkenylation reaction by the Ni(P(*i*-Pr)$_3$)/$AlMe_3$ catalyst are similar to those by Ni(NHC)/$AlMe_3$ catalyst except for several important differences, which will be discussed below; see Figures S14C and S15C and Tables S13 to S15. In the Ni(P(*i*-Pr)$_3$)/$AlMe_3$-catalyzed reactions, the electron population of the pyridine−$AlMe_3$ moiety increases much more in **TS2** of the C^2-alkenylation (0.154*e*) than in the C^4-one (0.141*e*), and it is the smallest in the C^3-alkenylation (0.121*e*). In **TS2** of the Ni(NHC)/$AlMe_3$-catalyzed reaction, the electron population of pyridine−$AlMe_3$ moiety is similar or slightly larger in C^2-alkenylation (0.131*e*) than in the C^4-one (0.124*e*) and it is smallest in the C^3-alkenylation (0.095*e*). These population changes in pyridine−$AlMe_3$ moiety suggest that the CT from Ni to pyridine−$AlMe_3$ is substantially larger in the C^2-alkenylation than in the C^4-alkenylation and it is smallest in the C^3-alkenyation by the Ni(P(*i*-Pr)$_3$)/$AlMe_3$ catalyst. These CT interactions from Ni to pyridine−$AlMe_3$ more stabilize **TS2** of the C^2-alkenylation than that of the C^4-alkenylation in the Ni(P(*i*-Pr)$_3$)/$AlMe_3$ catalyst. On the other hand, this stabilization of **TS2** by CT interaction is similar or slightly larger in the C^4-alkenylation than in the C^2-alkenylation by the Ni(NHC)/$AlMe_3$ catalyst.

In summary, both the steric effect and the electronic factor favor the C^2-alkenylation over the C^4-alkenylation in the Ni(P(*i*-Pr)$_3$)/$AlMe_3$ catalyst. Therefore, the C^2-alkenylation selectively occurs in the Ni(P(*i*-Pr)$_3$)/$AlMe_3$-catalyzed reaction unlike in the Ni(NHC)/$AlMe_3$-catalyzed one.

CONCLUDING REMARKS

In this theoretical study, we explored the regioselective alkenylation of pyridine by the Ni(NHC)/$AlMe_3$ cooperative catalyst to clarify the reaction mechanism, uncover the characteristic features of electronic processes of all elementary steps, and elucidate the factors determining the regioselectivity. The first step of the catalytic cycle is the coordination of pyridine−$AlMe_3$ with the active species $Ni^{(0)}(NHC)(C_2H_2)$ **1** in an η^2-fashion to form an intermediate **Int1**. **Int1** isomerizes to **Int2**, which undergoes the oxidative addition of the C−H bond of pyridine to the nickel−acetylene moiety to afford a Ni(II) pyridyl vinyl NHC complex **Int3**. This oxidative addition is understood to be the H^1-transfer from pyridine−$AlMe_3$ to the acetylene moiety, which is different from the usual transition state for the concerted oxidative addition. From **Int3**, acetylene coordination takes place to afford **Int4.** The final step is the reductive elimination of vinyl-pyridine product **P1**. The formation of butadienyl-pyridine product **P2** proceeds from **Int4** through the insertion of the second acetylene into the Ni−vinyl bond followed by the third acetylene coordination and the reductive elimination.

The oxidative addition of the C−H bond is the rate-determining step in the whole catalytic cycle. The $\Delta G^{\circ\ddagger}$ value for the C^2−H bond activation is the largest (22.1 kcal mol^{-1}), that for the C^3−H bond activation is the next (21.5 kcal mol^{-1}), and that for the C^4−H bond activation is the smallest (17.4 kcal mol^{-1}). These results agree with the experimental facts that the C^4-alkenylated pyridine−$AlMe_3$ is a major product, the C^3-alkenylated one is a minor, and the C^2 one is not formed. The selectivity was discussed with two factors: (i) the steric repulsion

DOI: 10.1021/acs.joc.6b02394
J. Org. Chem. 2017, 82, 289−301

between bulky *N*,*N*-diphenyl NHC ligand and $AlMe_3$ and (ii) the electronic factor for the C−H bond activation. It is concluded that the electronic factor facilitates the C^2- and C^4-alkenylations preferably to the C^3 one and the steric factor facilitates the C^3- and C^4-alkenylations. Thereby the C^4-alkenylation occurs selectively in the Ni(NHC)/$AlMe_3$-catalyzed reaction.

In the absence of $AlMe_3$, pyridine coordinates with the Ni atom through the N of pyridine to form a stable intermediate. As a result, the Gibbs activation energy ($\Delta G^{\circ\ddagger} = \sim 27$ kcal mol^{-1}) of the C−H bond activation increases. Also, the CT from Ni to pyridine is smaller in the absence of $AlMe_3$ than in the presence of $AlMe_3$. These are two important reasons why the alkenylation without Lewis acid is difficult.

In the alkenylation reaction by Ni(P(*i*-Pr)$_3$)/$AlMe_3$ catalyst, the steric effect is somewhat larger in the C^4-alkenylation than in the C^2-alkenylation. Also the electronic factor favors the C^2-alkenylation over the C^4-alkenylation in the Ni(P(*i*-Pr)$_3$)/$AlMe_3$-catalyzed reaction. As a result, the C^2-alkenylation selectively occurs in the Ni(P(*i*-Pr)$_3$)/$AlMe_3$-catalyzed reaction unlike in the Ni(NHC)/$AlMe_3$-catalyzed one. It is noted the $\Delta G^{\circ\ddagger}$ value for the second acetylene insertion into the Ni−vinyl bond (**TS4**) is smaller than the reductive elimination of **P1** (**TS3**), leading to the formation of C^2-substituted butadienyl pyridine product **P2**. These results arise from the smaller size of P(*i*-Pr)$_3$ than the NHC.

■ ASSOCIATED CONTENT

Supporting Information

The Supporting Information is available free of charge on the ACS Publications website at DOI: 10.1021/acs.joc.6b02394.

Geometry, energy, and NBO population changes, ONIOM details, basis set effects, translational entropy corrections, and Cartesian coordinates (PDF)

■ AUTHOR INFORMATION

Corresponding Authors

*E-mail: milind.deshmukh@gmail.com.

*E-mail: sakaki.shigeyoshi.47e@st.kyoto-u.ac.jp.

ORCID

Milind M. Deshmukh: 0000-0003-3518-7859

Notes

The authors declare no competing financial interest.

■ ACKNOWLEDGMENTS

Authors wish to thank University Grant Commission (UGC), New Delhi, for the start-up grant (No. F. 30-56/2014/BSR). S.S. is thankful for financial support by the Ministry of Education, Culture, Science, Sport and Technology through Grant-in-Aid "Stimuli-responsive Chemical Species for the Creation of Functional Molecules (No.2408)" (JSPS KAKENHI Grant No. JP15H00940), Grant-in-Aid for Scientific Research (JP15H03770), and Japan Science and Technology Cooperation (CREST "Establishment of Molecular Technology towards the Creation of New Functions" Area). Some of the computations were performed using Research Center for Computational Science, Okazaki, Japan. V.S. is thankful to Dr. Harisingh Gour University, Sagar, India, for research fellowship.

■ REFERENCES

(1) Daly, J. W.; Garraffo, H. M.; Spande, T. F. In *Alkaloids: Chemical and Biological Perspectives*; Pelletier, S. W., Ed.; Pergamon, New York, 1999; Vol. *13*, p 1−161.

(2) (a) Bosch, J.; Bennasar, M.-L. *Synlett* **1995**, 587−596. (b) Sinclair, A.; Stockman, R. A. *Nat. Prod. Rep.* **2007**, *24*, 298−326.

(3) (a) Su, R.; Wei, H.; Zhang, X.; Ma, S.; Yan, J.; Cui, Y.; Zhang, Z. *J. Heterocycl. Chem.* **2014**, *51*, 669−673. (b) Babu, S. S.; Praveen, V. K.; Ajayaghosh, A. *Chem. Rev.* **2014**, *114*, 1973−2129.

(4) Katritzky, A. R.; Taylor, R. *Adv. Heterocycl. Chem.* **1990**, *47*, 1−4.

(5) Katritzky, A. R.; Fan, W.-Q. *Heterocycles* **1992**, *34*, 2179−2229.

(6) Bull, J. A.; Mousseau, J. J.; Pelletier, G.; Charette, A. B. *Chem. Rev.* **2012**, *112*, 2642−2713.

(7) For some of the important references on the C−H bond activation of aromatic compounds, see: (a) Kakiuchi, F.; Murai, S. In *Activation of Unreactive Bonds and Organic Synthesis*; Murai, S., Ed.; Springer: Berlin, 1999; pp 47−79. (b) Li, J. J.; Gribble, G. W. *Palladium in Heterocyclic Chemistry*; Pergamon: Oxford, 2000; Chapter 4 and references therein. (c) Moore, E. J.; Pretzer, W. R.; O'Connell, T. J.; Harris, J.; La Bounty, L.; Chou, L.; Grimmer, S. S. *J. Am. Chem. Soc.* **1992**, *114*, 5888−5890. (d) Jordan, R. F.; Taylor, D. F. *J. Am. Chem. Soc.* **1989**, *111*, 778−779. (e) Ritleng, V.; Sirlin, C.; Pfeffer, M. *Chem. Rev.* **2002**, *102*, 1731−1770 and references therein.

(8) Murakami, M.; Hori, S. *J. Am. Chem. Soc.* **2003**, *125*, 4720−4721.

(9) Lewis, J. C.; Bergman, R. G.; Ellman, J. A. *J. Am. Chem. Soc.* **2007**, *129*, 5332−5333.

(10) Tobisu, M.; Hyodo, I.; Chatani, N. *J. Am. Chem. Soc.* **2009**, *131*, 12070−12071.

(11) Kawashima, T.; Takao, T.; Suzuki, H. *J. Am. Chem. Soc.* **2007**, *129*, 11006.

(12) Mukhopadhyay, S.; Rothenberg, G.; Gitis, D.; Baidossi, M.; Ponde, D. E.; Sasson, Y. *J. Chem. Soc., Perkin Trans. 2* **2000**, 1809−1812.

(13) Grigg, R.; Savic, V. *Tetrahedron Lett.* **1997**, *38*, 5737−5740.

(14) (a) Campeau, L.-C.; Rousseaux, S.; Fagnou, K. *J. Am. Chem. Soc.* **2005**, *127*, 18020−18021. (b) Leclerc, J.-P.; Fagnou, K. *Angew. Chem., Int. Ed.* **2006**, *45*, 7781−7786. (c) Kanyiva, K. S.; Nakao, Y.; Hiyama, T. *Angew. Chem., Int. Ed.* **2007**, *46*, 8872−8874.

(15) Nakao, Y.; Kanyiva, K. S.; Hiyama, T. *J. Am. Chem. Soc.* **2008**, *130*, 2448−2449.

(16) For review on C^2-, C^3-, and C^4-functionalization of pyridine, see: *Synthesis* **2011**, *20*, 3209−3219.

(17) Tsai, C.-C.; Shih, W.-C.; Fang, C.-H.; Li, C.-Y.; Ong, T.-G.; Yap, G. P. A. *J. Am. Chem. Soc.* **2010**, *132*, 11887−11889.

(18) Nakao, Y.; Yamada, Y.; Kashihara, N.; Hiyama, T. *J. Am. Chem. Soc.* **2010**, *132*, 13666−13668.

(19) For C^3-selective catalytic C−C bond formation with pyridines, see: (a) Ye, M.; Gao, G.-L.; Edmunds, A. J. F.; Worthington, P. A.; Morris, J. A.; Yu, J.-Q. *J. Am. Chem. Soc.* **2011**, *133*, 19090−19093. (b) Ye, M.; Gao, G.-L.; Yu, J.-Q. *J. Am. Chem. Soc.* **2011**, *133*, 6964−6967.

(20) For Ir-catalyzed C^3-selective catalytic C−C bond formation with pyridines, see: (a) Li, B.-J.; Shi, Z.-J. *Chem. Sci.* **2011**, *2*, 488−493. (b) Hartwig, J. F. *Chem. Soc. Rev.* **2011**, *40*, 1992−2002.

(21) For the C^4-selective catalytic alkenylation/alkylation of pyridines, see: (a) Andou, T.; Saga, Y.; Komai, H.; Matsunaga, S.; Kanai, M. *Angew. Chem.* **2013**, *125*, 3295−3298.

(22) Oshima, K.; Ohmura, T.; Suginome, M. *J. Am. Chem. Soc.* **2011**, *133*, 7324−7327.

(23) (a) Bair, J. S.; Schramm, Y.; Sergeev, A. G.; Clot, C.; Eisenstein, O.; Hartwig, J. F. *J. Am. Chem. Soc.* **2014**, *136*, 13098−13101. (b) Guihaumé, J.; Halbert, S.; Eisenstein, O.; Perutz, R. N. *Organometallics* **2012**, *31*, 1300−1314.

(24) Guan, W.; Sakaki, S.; Kurahashi, T.; Matsubara, S. *ACS Catal.* **2015**, *5*, 1−10.

(25) (a) Vastine, B. A.; Hall, M. B. *J. Am. Chem. Soc.* **2007**, *129*, 12068−12069. (b) Ess, D. H.; Goddard, W. A., III; Periana, R. A. *Organometallics* **2010**, *29*, 6459−6472.

(26) (a) Becke, A. D. *Phys. Rev. A: At., Mol., Opt. Phys.* **1988**, *38*, 3098−3100. (b) Becke, A. D. *J. Chem. Phys.* **1993**, *98*, 5648−5652.

(27) Perdew, J. P.; Wang, Y. *Phys. Rev. B: Condens. Matter Mater. Phys.* **1992**, *45*, 13244−13249.

(28) (a) Hariharan, P. C.; Pople, J. A. *Theor. Chim. Acta.* **1973**, *28*, 213−222. (b) Francl, M. M.; Pietro, W. J.; Hehre, W. J.; Binkley, J. S.;

DOI: 10.1021/acs.joc.6b02394
J. Org. Chem. 2017, 82, 289−301

Gordon, M. S.; DeFrees, D. J.; Pople, J. A. *J. Chem. Phys.* **1982**, *77*, 3654−3665.
(29) (a) Hay, P. J.; Wadt, W. R. *J. Chem. Phys.* **1985**, *82*, 270−283. (b) Wadt, W. R.; Hay, P. J. *J. Chem. Phys.* **1985**, *82*, 284−298. (c) Hay, P. J.; Wadt, W. R. *J. Chem. Phys.* **1985**, *82*, 299−310.
(30) (a) Bergner, A.; Dolg, M.; Kuechle, W.; Stoll, H.; Preuss, H. *Mol. Phys.* **1993**, *80*, 1431−1441. (b) Kaupp, M.; Schleyer, P. v. R.; Stoll, H.; Preuss, H. *J. Chem. Phys.* **1991**, *94*, 1360−1366. (c) Dolg, M.; Stoll, H.; Preuss, H.; Pitzer, R. M. *J. Phys. Chem.* **1993**, *97*, 5852−5859.
(31) (a) Grimme, S.; Antony, J.; Ehrlich, S.; Krieg, H. *J. Chem. Phys.* **2010**, *132*, 154104. (b) The dispersion corrected B3LYP-D3 functional is employed because the steric repulsion between the ligand and Lewis acid is one of the important factors which affect the energetics of reactions and hence the regioselectivity of the product. Also, we recalculated the Gibbs activation barrier for the rate-determining step with various functionals; see p S24 and Table S8A. The present results at the B3LYP-D3/BS-II level are in good agreement with those at the M06/BS-II level, recommended in the earlier works (see refs 24 and 34) of Ni/LA-catalyzed reactions.. (c) The basis set effect were also examined; see p S25 and Table S8B.
(32) Frisch, M. J.; et al. *Gaussian 09*, revision B.01; Gaussian, Inc.: Wallingford, CT, 2010; see Supporting Information p S43 for complete reference.
(33) (a) Barone, V.; Cossi, M. J. *J. Phys. Chem. A* **1998**, *102*, 1995. (b) Cossi, M.; Rega, N.; Scalmani, G.; Barone, V. J. *J. Comput. Chem.* **2003**, *24*, 669. (c) Tomasi, J.; Mennucci, B.; Cammi, R. *Chem. Rev.* **2005**, *105*, 2999−3093. (d) Mammen, M.; Shakhnovich, E. I.; Deutch, J. M.; Whitesides, G. M. *J. Org. Chem.* **1998**, *63*, 3821−3830.
(34) (a) Guan, W.; Sayyed, F. B.; Zeng, G.; Sakaki, S. *Inorg. Chem.* **2014**, *53*, 6444−6457. (b) Sakaki, S. *Bull. Chem. Soc. Jpn.* **2015**, *88*, 889−938.
(35) The reductive elimination of product **P1** is also possible starting from **Int3a**. In this step, **Int3a** isomerizes to the more stable **Int3a′** (by −6.07 kcal mol^{-1}) via vinyl rotation ($\Delta G^{\circ\ddagger}_{rot.}$ = 8.3 kcal mol^{-1}) followed by the reductive elimination from **Int3a′** with an activation barrier of 8.7 kcal mol^{-1}; see p S44. This step of vinyl rotation is very similar to that discussed by Eisenstein et al; see ref 23.
(36) We also investigated the reductive elimination of product **P2** starting from **Int5a**. In this step, **Int5a** isomerizes to the more stable **Int5a′** (by −6.75 kcal mol^{-1}) via butadienyl rotation ($\Delta G^{\circ\ddagger}_{rot.}$ = 6.8 kcal mol^{-1}) followed by the reductive elimination from **Int5a′** with an activation barrier of 8.2 kcal mol^{-1}; See p S45. The step of vinyl rotation is very similar to that discussed by Eisenstein et al; see ref 23.
(37) For instance: (a) Sakaki, S.; Ieki, M. *J. Am. Chem. Soc.* **1993**, *115*, 2373−2381. (b) Sakaki, S.; Mizoe, N.; Musashi, Y.; Biswas, B.; Sugimoto, H. *J. Phys. Chem. A* **1998**, *102*, 8027−8036. (c) Ochi, N.; Nakao, Y.; Sato, H.; Sakaki, S. *J. Am. Chem. Soc.* **2007**, *129*, 8615−8624.
(38) The Gibbs energy was not considered in the ONIOM calculation because the model as well as the real substituent structures were taken from corresponding real and model complexes without geometry optimization; in other words, vibration movement cannot be evaluated. The trend in the Gibbs energy barrier for model complex and that of the real system agree with that in electronic energy; see Table S9 and Table 3.

DOI: 10.1021/acs.joc.6b02394
J. Org. Chem. 2017, 82, 289−301